Synthesis of stable and low-Co2 selective Ɛ-iron carbide Fischer-Tropsch catalysts

Wang, Peng; Chen, Wei; Chiang, Fu-Kuo; Dugulan, Iulian; Song, Yuanjun; Pestman, Robert; Zhang, Kui; Yao, Jinsong; Feng, Bo; Miao, Ping

DOI
10.1126/sciadv.aau2947

Publication date
2018

Published in
Science Advances

CHEMISTRY

Synthesis of stable and low-CO_2 selective ε-iron carbide Fischer-Tropsch catalysts

Peng Wang[1,2]*, Wei Chen[2]*, Fu-Kuo Chiang[1], A. Iulian Dugulan[3], Yuanjun Song[4], Robert Pestman[2], Kui Zhang[1], Jinsong Yao[1], Bo Feng[1], Ping Miao[1], Wayne Xu[1], Emiel J. M. Hensen[2]†

The Fe-catalyzed Fischer-Tropsch (FT) reaction constitutes the core of the coal-to-liquids (CTL) process, which converts coal into liquid fuels. Conventional Fe-based catalysts typically convert 30% of the CO feed to CO_2 in the FT unit. Decreasing the CO_2 release in the FT step will reduce costs and enhance productivity of the overall process. In this context, we synthesize phase-pure ε(′)-Fe_2C catalysts exhibiting low CO_2 selectivity by carefully controlling the pretreatment and carburization conditions. Kinetic data reveal that liquid fuels can be obtained free from primary CO_2. These catalysts displayed stable FT performance at 23 bar and 235°C for at least 150 hours. Notably, in situ characterization emphasizes the high durability of pure ε(′)-Fe_2C in an industrial pilot test. These findings contribute to the development of new Fe-based FT catalysts for next-generation CTL processes.

INTRODUCTTION

Coal is so far the most plentiful fossil resource, nearly four times more abundant than petroleum or natural gas (*1*, *2*). Efficient use of coal is pivotal to domestic economies that are rich in coal. For instance, China represents the largest coal market in the world and is expanding its coal-to-liquids (CTL) technology by ~2% per year. By 2020, CTL is expected to account for 15% of the coal use in China (*3*). Accordingly, there is a large incentive to improve current CTL technology, which can convert coal into liquid fuels and valuable chemicals (*4*, *5*). The CTL process consists of four stages, namely, synthesis gas production by coal gasification, the water-gas shift (WGS) reaction, Fischer-Tropsch (FT) synthesis (*6*–*9*), and product upgrading. In the context of coal-based FT synthesis, Fe-based catalysts are preferred over Co-based ones due to their tolerance to sulfur, low cost, and high operational flexibility (*10*, *11*). A well-known issue with Fe-based catalysts is that they typically convert 30% of the CO reactant to CO_2 as a by-product instead of nearly exclusively H_2O as for Co (*7*, *8*, *12*).

Considering the oxygen balance of the overall CTL process, oxygen is introduced as H_2O and O_2 during synthesis gas production (coal gasification) and is eventually removed as CO_2 in the WGS and as CO_2 and H_2O in the FT synthesis section (*9*, *12*). Although the total amount of CO_2 (WGS + FT) to be released is a constant (see the supplementary materials for mass balance calculation), the amount of CO_2 produced in the FT synthesis reactor not only decreases CO conversion, therefore requiring a higher recycle rate to obtain high overall CO conversion, but also occupies part of the gas holdup of the CTL plant, leading to additional energy consumption for heating, compression, and separation (*7*–*9*, *13*). Taking into account these aspects, we estimated the annual energy consumption as a function of the CO_2 selectivity in the FT reaction (excluding as a first approximation CO_2 from the WGS reaction; see the supplementary materials for calculation). Figure 1 shows that eliminating CO_2 formation in the FT reactor can substantially cut operational cost. Eliminating CO_2 production in the FT reactor implies that all CO_2 is generated in the WGS reactor. This is meaningful as concentrated production of CO_2 will make its removal more feasible, which is important for carbon capture and storage/utilization strategies in the context of clean CTL technologies (*14*, *15*). Thus, it is worthwhile to develop an Fe-based FT catalyst with an as low as possible CO_2 selectivity.

The complexity of Fe-based FT catalysts hinders the development of improved materials with a low CO_2 selectivity (*6*, *8*, *12*, *16*, *17*). Depending on catalyst pretreatment, these catalysts may contain metallic iron, iron oxide, and iron carbides. In particular, the latter are thought to be crucial for FT performance, and several iron carbides such as χ-Fe_5C_2, θ-Fe_3C, ε(′)-$Fe_{2(.2)}C$, and Fe_7C_3 have been identified as active components for the FT reaction (*18*–*21*). de Smit

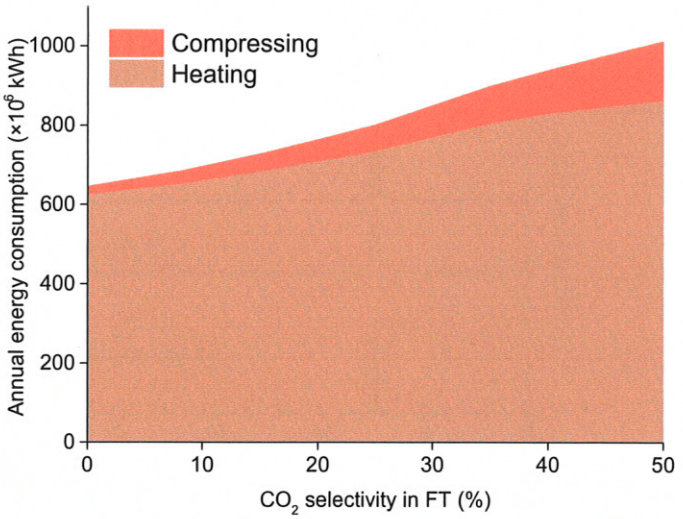

Fig. 1. The influence of the CO_2 selectivity in the FT reaction on the annual (8000 hours per year) energy consumption of a 500 kton $year^{-1}$ liquid fuel production FT plant (including reactor, heater, compressor, and separator).

[1]National Institute of Clean-and-Low-Carbon Energy, Shenhua NICE, Future Science and Technology City, Changping District, Beijing 102211, People's Republic of China. [2]Laboratory of Inorganic Materials Chemistry, Schuit Institute of Catalysis, Department of Chemical Engineering and Chemistry, Eindhoven University of Technology, P.O. Box 513, 5600 MB Eindhoven, Netherlands. [3]Fundamental Aspects of Materials and Energy Group, Delft University of Technology, 2629 JB Delft, Netherlands. [4]Beijing Key Laboratory for Magneto-Photoelectrical Composite and Interface Science, School of Mathematics and Physics, University of Science and Technology Beijing, Beijing 100083, People's Republic of China.
*These authors contributed equally to this work.
†Corresponding author. Email: e.j.m.hensen@tue.nl

et al. (*19*, *20*) studied the stability and phase transformation of these carbide phases as a function of the carbon chemical potential. With the aim of studying their contribution to the FT reaction, several efforts have been made to synthesize phase-pure iron carbides. Ma and co-workers (*22*) introduced bromide to prepare χ-Fe_5C_2 nanoparticles. Santos and co-workers (*23*) achieved highly dispersed χ-Fe_5C_2 with 86% purity by means of a metal organic framework-mediated synthesis. The CO_2 selectivity at 340°C, 20 bar, $H_2/CO = 1$, and a GHSV (gas hourly space velocity) of 30,000 $hour^{-1}$ of this material is about 47%, which is close to the theoretical upper limit of 50%. Xu *et al.* (*24*) recently showed that a catalyst containing 73% ε-iron carbide has a promising activity and a relatively low CO_2 selectivity (20%) at 200°C. An important corollary of these and other studies is that it is challenging to prepare phase-pure iron carbides. Another aspect is that it is usually assumed that ε-iron carbides will easily transform into the more stable Hägg carbide (χ-Fe_5C_2) during the FT reaction (*20*, *25*–*27*).

RESULTS AND DISCUSSION

In this work, we present a novel synthetic procedure to obtain pure ε(′)-carbide by carefully controlling the pretreatment and carburization conditions. The approach consists of (i) fully reducing iron oxide to iron metal in a H_2 flow, (ii) pretreating the metal precursor in dilute synthesis gas ($H_2/CO/N_2 = 2/1/10$) at 170°C for 40 min, and (iii) slowly ramping this precursor to 250°C at a rate of 0.5°C min^{-1} in synthesis gas with a $H_2/CO/N_2 = 3/2/2$ composition for 6 hours (see the supplementary materials for details). The reduction temperature of the first step depends on the iron oxide precursor, while the latter two constitute the carburization step. Notably, this approach can be applied to any reducible iron precursor, avoiding the use of expensive or toxic chemicals. Moreover, its simplicity means that we can carry out this procedure in different types of reactors including an in situ reactor device for Mössbauer spectroscopy characterization and an industrial pilot-scale reactor. To showcase our approach, we prepared an unsupported catalyst using Raney-Fe as a starting material (denoted as R-Fe) and a silica-supported Fe catalyst (Fe/SiO_2). Preparation methods are available in the supplementary materials. The resulting ε(′)-carbide catalysts show an unexpected stability and unprecedented low CO_2 selectivity in the FT reaction. Although the FT performance of the two catalysts differs slightly due to the different physicochemical properties, their kinetic performance is sufficiently similar to conclude that the active phases are the same. Therefore, in the rest of this work, we focus on the R-Fe catalyst. Corresponding data for the Fe/SiO_2 catalyst are collected in the supplementary materials (figs. S1 to S3).

We note here that ε-Fe_2C and ε′-$Fe_{2.2}C$ share the same space group [$P6_3/mmc$ (194)] and cell dimensions, with carbon occupying the same octahedral interstices (O-carbides) in slightly different concentrations. Therefore, these phases show very similar chemical properties and are often considered as one phase, denoted hereafter as ε(′)-carbide (*20*, *24*, *28*). The in situ x-ray diffraction (XRD) pattern of the reduced sample (black line in Fig. 2A) indicates the completeness of iron reduction. After pretreatment at 170°C in synthesis gas with $H_2/CO = 2$, the XRD pattern hardly changes, implying that the metallic iron phase is maintained (blue line in Fig. 2A). On the other hand, the temperature-programmed hydrogenation (TPH) profile of the pretreated sample (blue line in Fig. 2B) reveals that surface carbon was deposited on the metallic iron surface. This type of carbon can be hydrogenated to methane at 350°C. As the intensities of the metallic iron component in the pretreated sample are hardly affected by the exposure to synthesis gas, we conclude that most of the deposited carbon remains on the surface and it does not lead to bulk iron carbides. In situ XRD after the carburization shows that phase-pure ε(′)-carbide was obtained (PDF#36-1249). The TPH profile contains the typical characteristic peaks of carbon species in ε(′)-carbide in line with an earlier study (*29*). Operando Mössbauer spectra (Fig. 3) following the same procedure confirm that the as-synthesized catalyst is made up exclusively of ε(′)-carbide (detailed spectral interpretation in the supplementary materials). The Mössbauer spectroscopy measurements also demonstrate that the formed ε(′)-carbide can survive industrially relevant FT synthesis conditions.

In the course of our investigations, we found that it is essential to fully reduce the iron precursor before the pretreatment steps. Otherwise, the final catalyst will be composed of a mixture of iron oxide and iron carbide, as usually observed in conventional Fe-based FT

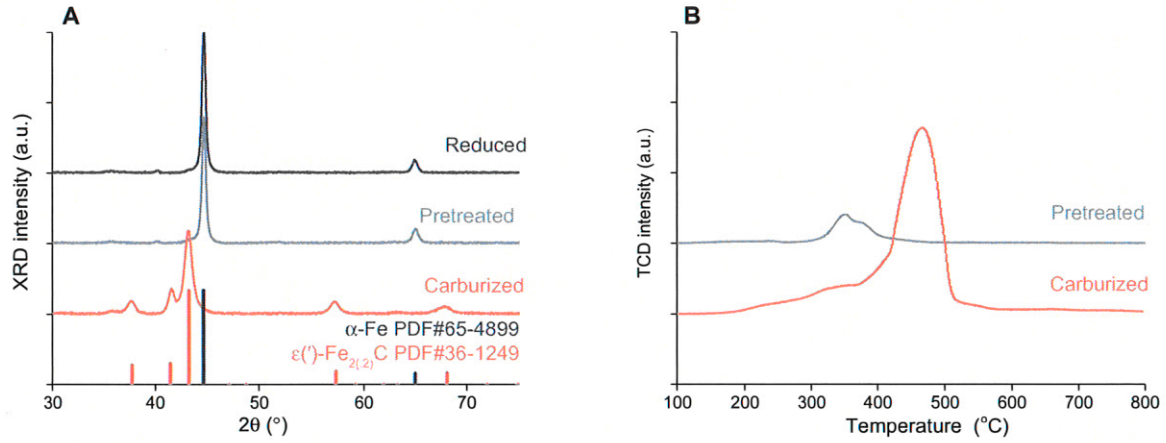

Fig. 2. Investigation of ε(′)-carbide formation. (**A**) In situ XRD patterns of reduced (black), pretreated (blue), and carburized (red) R-Fe catalyst. a.u., arbitrary units. (**B**) TPH profiles of pretreated (blue) and carburized (red) R-Fe catalyst. Carbide synthesis procedure: (i) reduction: H_2 flow, 1 bar, 430°C, 1 hour; (ii) pretreatment: $H_2/CO = 2$, 1 bar, 170°C, isothermal period of 40 min; (iii) carburization: $H_2/CO = 1.5$, 1 bar, ramping from 170° to 250°C at a rate of 0.5°C min^{-1}, isothermal period of 1 hour. TCD, thermal conductivity detector.

catalysts. In situ XRD patterns (fig. S4) show that Fe_3O_4 cannot be carburized in synthesis gas at 250°C. Mössbauer spectra confirm that carburization of Fe_3O_4 hardly proceeds and will only lead to χ-carbide (fig. S5), which is thermodynamically favored over ε(′)-carbide under FT conditions. We also found by using in situ XRD (fig. S6) that carburization of metallic Fe particles larger than 30 nm results in a mixture of ε(′)-carbide and χ-carbide. We speculate that this is due to an insufficient carbon diffusion rate in large metallic Fe particles during the carburization step. The Fe particles of the R-Fe and Fe/SiO_2 catalysts used in longer-term FT tests, which will be discussed later, have an average particle size of 27 and 19 nm, respectively. We should also highlight the importance of exposure to synthesis gas at relatively low temperature. Without this step, again, a mixture of ε(′)-carbide and χ-carbide will be obtained as confirmed by XRD (fig. S7). This signifies the importance of the carbon species formed during the pretreatment step to ε(′)-carbide formation. During carburization, there is a competition of carbon atoms for bulk phase diffusion, hydrogenation, and graphitic carbon formation. As it has been reported that the formation of ε(′)-carbide phase requires low temperature and high carbon chemical potential (*20*), we speculate that predeposited carbon may deactivate the surface sufficiently to facilitate the formation of ε(′)-carbide over χ-carbide.

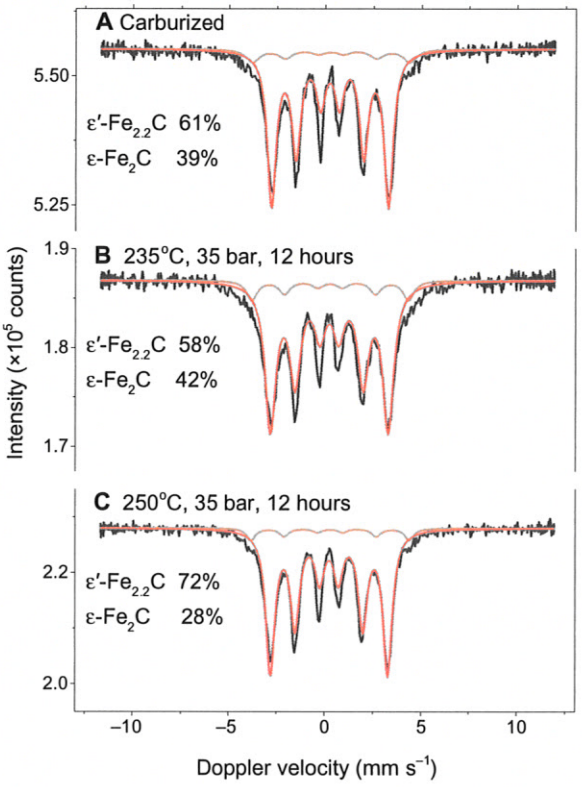

Fig. 3. Operando Mössbauer spectroscopy of R-Fe catalysts. (**A**) Pretreated at $H_2/CO = 2$, 1 bar, 170°C for 40 min, followed by ramping to 250°C at a rate of 0.5°C min^{-1}, dwelling for 1 hour; (**B**) $H_2/CO = 1.5$, 23 bar, 235°C for 12 hours; (**C**) $H_2/CO = 1.5$ with saturated vapor water at 35°C, 23 bar, 250°C for 12 hours. Mössbauer data were acquired at 4.2 K.

To study the carburization process in more detail, we used environmental transmission electron microscopy (TEM). Figure 4A shows high-resolution TEM (HRTEM) images of a single crystal after carburization for 20 min. The fast Fourier transform (FFT) of the selected area in Fig. 4A emphasizes that the large crystal consists of two different structures. The FFT in Fig. 4B is composed of inner and outer symmetric spots belonging to lattice spacings of 2.1 Å (blue circle) and 2.0 Å (red circle), representing Fe(110) and ε-Fe_2C(101) planes, respectively. The mismatch angle of 4.7° between the inner and outer spots indicates the tilting angle between these two planes in the crystal. The filtered image in real space as shown in Fig. 4C represents the inverse FFT (IFFT) of the selected area in Fig. 4A (dashed square). According to the spacing of lattice fringes, Fe is located near the core of the crystal (right side of Fig. 4C) and ε-Fe_2C on the surface (interface indicated by the dash-dot line). Some dislocations are observed at the interface (marked by "T" in Fig. 4C), where extra rows are visible in the Fe phase to compensate the lattice mismatch. By selecting deflection spots in Fig. 4B, the distribution of Fe (Fig. 4D) and ε-Fe_2C (Fig. 4E) can be

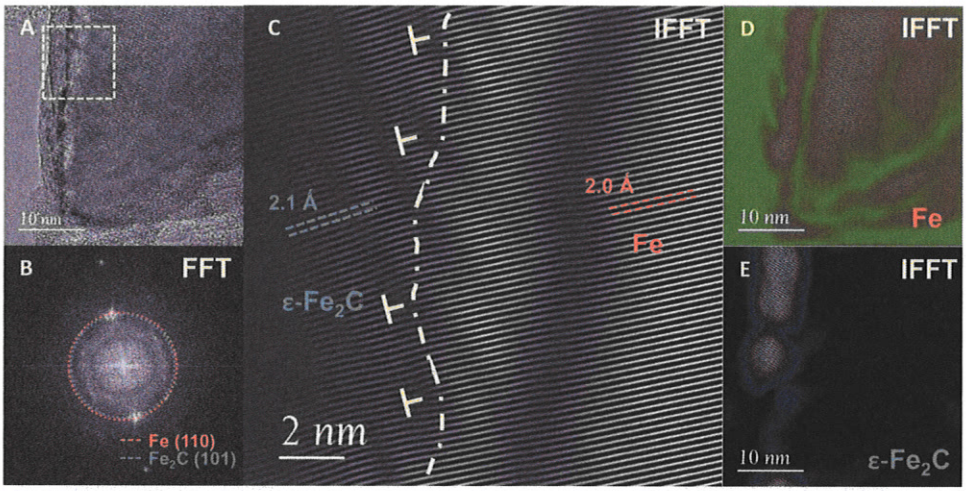

Fig. 4. Observation of ε(′)-carbide formation by environmental TEM. A well-ground sample was in situ reduced in a H_2 flow at 430°C for 20 hours. Subsequently, the sample was exposed to a synthesis gas flow ($H_2/CO = 2.4/1.2$) at 170°C for 20 min. During this dwell, HRTEM images were taken. (**A**) HRTEM image. (**B**) FFT of selected area. (**C**) IFFT image. (**D**) IFFT image of α-Fe. (**E**) IFFT image of ε-Fe_2C.

highlighted in real space, suggesting that ε-Fe_2C grows epitaxially on the surface of Fe.

Catalytic tests were performed in a fixed-bed reactor under typical industrial conditions, namely, at 235°C, a H_2/CO ratio of 1.5, a pressure of 35 bar, and a GHSV of 18,000 $hour^{-1}$. Most attractively, the CO_2 selectivity is as low as 5% (Fig. 5A), which is significantly lower than values reported for conventional Fe-based catalysts under similar conditions (*8*, *12*, *30*, *31*). As discussed earlier, a low CO_2 selectivity in FT synthesis will reduce operational expenditure and increase plant productivity. Note that the activity of the R-Fe catalyst is remarkably stable during 150-hour time on stream at a CO conversion of approximately 15%. Usually, it is assumed that ε(′)-carbide phases are not stable under FT conditions with respect to χ-carbide (*20*). To gain an insight into this apparent contradiction, we used operando Mössbauer spectroscopy to monitor the phase composition of the R-Fe catalyst at reaction conditions. Considering the fact that the CO conversion operando Mössbauer cell is limited by mass transport, we saturated the synthesis gas into a water saturator [partial pressure of water (P_{H_2O}) = 97.8 mbar] to mimic the water partial pressure under practical FT synthesis conditions. After 12-hour reaction at 235°C, the catalyst is composed of 88% ε′-$Fe_{2.2}C$ and 12% ε-Fe_2C (Fig. 3B), indicative of the good stability of the ε(′)-carbide phases. To evaluate whether the formed ε(′)-carbide is also stable at higher temperature, we increased the reaction temperature from 235° to 250°C for 25 hours, followed by a decrease to 235°C. Figure 4B shows that the CO conversion and CO_2 selectivity were higher at 250°C and regained their original values after the temperature was lowered to 235°C. This suggests that the phase composition does not change during this temperature excursion, which is confirmed by a similar experiment carried out in the operando Mössbauer spectroscopy cell (Fig. 3C). In summary, the catalytic tests and operando Mössbauer spectroscopy characterization reveal that the low and stable CO_2 formation rate is related to the good thermal stability of ε(′)-carbide at industrially relevant conditions.

Using this phase-pure ε(′)-carbide catalyst, we could gain further insight into CO_2 formation in the FT synthesis reaction. Figure 6 shows the CO_2 selectivity as a function of the CO conversion, which was varied by changing the total flow rate at constant H_2/CO ratio. Earlier, it has been concluded that CO_2 formation on Fe-based FT catalysts is composed of primary CO_2 and secondary CO_2 (*32*). The primary CO_2 selectivity can be obtained by extrapolating the CO_2 selectivity to zero CO conversion. The rest is assigned to secondary CO_2, whose selectivity increases with CO conversion and reflects the re-adsorption of H_2O as the primary O removal product and its reaction with CO to CO_2 via the WGS reaction (*32*). As shown in Fig. 6, the ε(′)-carbide catalyst is free of primary CO_2, implying that the O atoms released by CO dissociation are exclusively removed as H_2O. We contrast our result with an earlier study (*30*, *32*), which shows a primary CO_2 selectivity of 7 to 15% at comparable conditions. The increasing CO_2 selectivity at higher CO conversion is therefore due to the WGS reaction of CO reactant with the primary H_2O product (*12*). Conventional Fe-based FT catalysts are a mixture of metallic iron, iron oxides, and carbides, producing both primary and secondary CO_2 (*19*, *30*, *31*). Considering the absence of primary CO_2 on our phase-pure ε(′)-carbide catalyst, we relate the formation of CO_2 as a primary product to the presence of metallic iron or iron oxides. As metallic iron is seldom observed in active Fe-based FT catalysts, we can attribute primary CO_2 formation to iron oxides present in conventional Fe FT catalysts (*33*, *34*). This is consistent with iron oxides being the main phase in commercial WGS catalysts. We point out that secondary CO_2 formed via the WGS reaction in the FT reactor strongly depends on the H_2O partial pressure in the FT reactor. Accordingly, it can be controlled to some extent by the way the reaction is carried out.

CONCLUSION

In summary, we present in this work a universally applicable synthesis method of pure ε(′)-carbide catalyst synthesis. Some key issues of the successful synthesis are studied by in situ and operando characterization. The stability and low CO_2 selectivity of the ε(′)-carbide catalysts under industrial FT conditions show its potential for practical application. This scalable method for preparing highly selective Fe-based FT catalysts will also facilitate the development of new catalysts for intensified CTL processes and provide a starting point for more detailed studies of the catalytic nature of Fe-based FT synthesis.

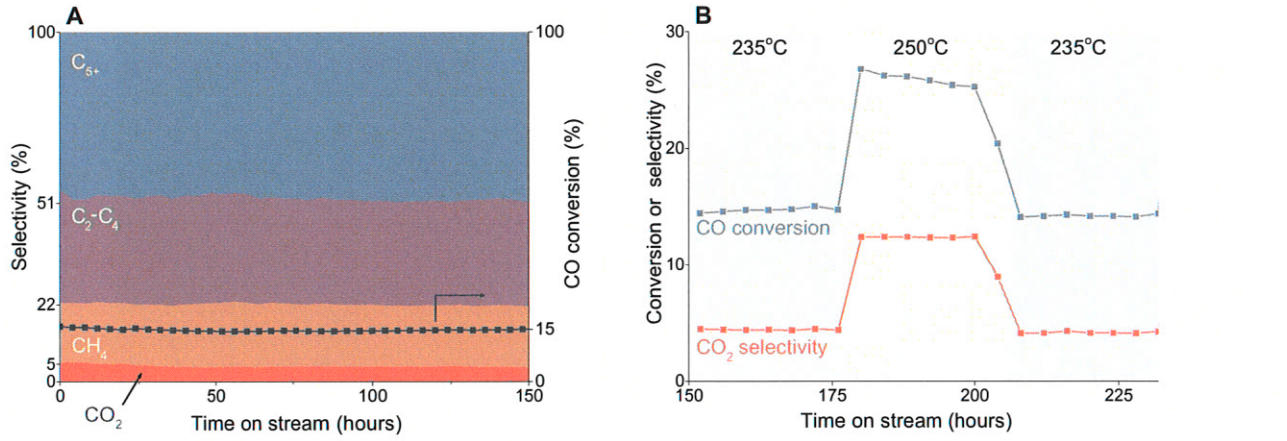

Fig. 5. FT performance of the R-Fe catalyst as a function of time on stream. (**A**) H_2/CO = 1.5, 23 bar, 235°C, GHSV of 18,000 $hour^{-1}$. (**B**) After 175-hour time on stream, the reaction temperature was increased to 250°C and kept there for 24 hours followed by a decrease to 235°C.

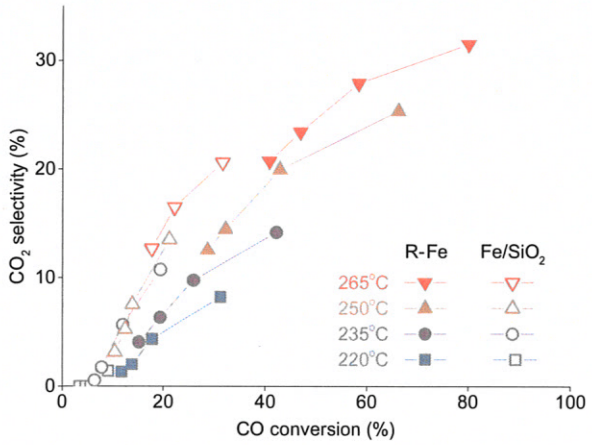

Fig. 6. CO_2 selectivity as a function of CO conversion on R-Fe (solid) and Fe/SiO_2 (open) catalysts at different temperatures. The CO conversion is varied by adjusting the flow rate at a constant H_2/CO ratio.

MATERIALS AND METHODS

Materials

R-Fe–based catalyst

Fe/Al alloy powder (50:50 by weight, 200 mesh; Hu'nan Xingyuan Powder Co.) was added into 8 M KOH (AR, Sinopharm Chemical Reagent Co.) solution in a flask under stirring and heated to 70° ± 1°C to dissolve Al in the alloy. Afterward, K^+ and AlO_2^- ions in the solution were washed away sequentially by deionized water (10 times) and ethanol (7 times). The Fe sample powder was transferred into a sealable quartz tube in a glove box and subsequently dried in an Ar flow at room temperature for 6 hours. As-prepared porous Fe powder was kept in a glove box with an extra seal. Before loading the sample in the in situ XRD cell, the in situ Mössbauer cell, or the FT reactor, the sample was passivated in a flow of 1% O_2 in He at room temperature for 20 hours.

Fe/SiO_2 catalyst

SiO_2-supported Fe sample was prepared by incipient wetness impregnation method with SiO_2 support (Q15, 120 mesh; Sasol) using an aqueous solution of $Fe(NO_3)_3{\cdot}9H_2O$ (AR, Sinopharm Chemical Reagent Co.). The sample was sequentially dried at 80°C for 12 hours and 120°C for 24 hours and then calcined at 500°C for 5 hours in static air.

Characterization

In situ XRD

In situ XRD was carried out on a Rigaku D/max-2600/PC apparatus equipped with a D/teX Ultra high-speed detector and scintillation counter. The x-ray generator consisted of a Cu rotating anode target with a maximum power of 9 kW. All the tests were operated at 40 mA and 40 kV. In situ XRD patterns were recorded in an Anton Paar XRK-900 cell equipped with a CO/H_2/inert gas inlet system.

Temperature-programmed hydrogenation

TPH was conducted in a quartz tube reactor equipped with a mass spectrometer. Typically, 50 mg of the sample was in situ reduced and carburized before the TPH experiment. During the TPH, the temperature was increased from room temperature to 750°C at a rate of 5°C min^{-1} in a dilute H_2 flow (20% H_2 in He, 50 ml min^{-1} in total).

Environmental TEM

Environmental TEM images were recorded in an aberration-corrected FEI Titan ETEM G2 instrument at an acceleration voltage of 300 kV. A well-ground sample was in situ reduced in a H_2 flow (10 mbar) at 430°C for 20 hours. After reduction, a syngas feed (H_2/CO = 2, 3 mbar) was admitted to pass through the sample at 170°C and kept for 2 hours. The HRTEM was taken in situ during the process above.

Operando Mössbauer spectroscopy

Operando Mössbauer spectroscopy was carried out in a state-of-the-art high-pressure Mössbauer cell (*35*). Transmission ^{57}Fe Mössbauer spectra were collected at 4.2 K (liquid helium) with a sinusoidal velocity spectrometer using a ^{57}Co(Rh) source. The source and the absorbing samples were kept at the same temperature during the measurements. MossWinn 4.0 software was used for spectra fitting (*36*). Detailed fitting parameters (tables S2 to S4) and discussion (section S3) are provided in the supplementary materials.

Carbide synthesis and catalytic tests

In each run, 500 mg of the catalyst precursor diluted with 3 g of quartz sand was loaded in a stainless steel tubular fixed-bed reactor. The catalyst precursor was in situ reduced in H_2 flow (20% H_2 in N_2; ambient pressure, 3750 ml·g_{cat}^{-1}·$hour^{-1}$) at 280°C for 12 hours for the R-Fe sample and at 430°C for 24 hours for the SiO_2-supported Fe sample. The reactor was then cooled to 170°C. Subsequently, the sample was pretreated in a dilute syngas (16% H_2/8% CO/76% N_2; ambient pressure, 1.875 liters $hour^{-1}$) for 40 min. Thereafter, we adjusted the composition of syngas to 43% H_2/28.5% CO/28.5% N_2 and increased the flow rate to 5.25 liters $hour^{-1}$. Meanwhile, the temperature was increased to 250°C at a rate of 0.5°C min^{-1} and kept for 6 hours to carburize the sample further. After that, the reactor was cooled to 235°C and pressurized to 23 bar to start the FT synthesis reaction. The effluent gas flow was analyzed online by Agilent 7890 GC equipped with two thermal conductivity detectors and one flame ionization detector.

SUPPLEMENTARY MATERIALS

Supplementary material for this article is available at http://advances.sciencemag.org/cgi/content/full/4/10/eaau2947/DC1

Section S1. Mass balance calculation
Section S2. Energy consumption calculation
Section S3. Operando Mössbauer spectroscopy
Scheme S1. Model of an FT plant.
Table S1. FT plant modeling as a function of CO_2 selectivity in FT reactor.
Table S2. Fitting parameters of the Mössbauer spectra of R-Fe catalyst.
Table S3. Fitting parameters of the Mössbauer spectra of Fe/SiO_2 catalyst.
Table S4. Fitting parameters of the Mössbauer spectra of insufficiently reduced R-Fe catalysts.
Fig. S1. In situ XRD patterns of the Fe/SiO_2 catalyst throughout the ε(′)-carbide synthesis procedure.
Fig. S2. Operando Mössbauer spectra of Fe/SiO_2 catalyst.
Fig. S3. FT performance of Fe/SiO_2 catalyst containing only ε(′)-carbide as a function of time on stream.
Fig. S4. In situ XRD patterns of the R-Fe catalyst throughout the ε(′)-carbide formation.
Fig. S5. Operando Mössbauer spectra of insufficiently reduced R-Fe catalyst recorded in different stages.
Fig. S6. In situ XRD patterns of various samples sequentially treated by reduction and carburization.
Fig. S7. In situ XRD patterns of the R-Fe catalysts synthesized following different procedures.
References (*37*–*39*)

REFERENCES AND NOTES

1. J. Chow, R. J. Kopp, P. R. Portney, Energy resources and global development. *Science* **302**, 1528–1531 (2003).
2. D. P. Schrag, Preparing to capture carbon. *Science* **315**, 812–813 (2007).
3. International Energy Agency, *World Energy Outlook 2014* (International Energy Agency, 2014).
4. F. Jiao, J. Li, X. Pan, J. Xiao, H. Li, H. Ma, M. Wei, Y. Pan, Z. Zhou, M. Li, S. Miao, J. Li, Y. Zhu, D. Xiao, T. He, J. Yang, F. Qi, Q. Fu, X. Bao, Selective conversion of syngas to light olefins. *Science* **351**, 1065–1068 (2016).

5. S. Chu, A. Majumdar, Opportunities and challenges for a sustainable energy future. *Nature* **488**, 294–303 (2012).
6. F. Fischer, H. Tropsch, The preparation of synthetic oil mixtures (synthol) from carbon monoxide and hydrogen. *Brennst. Chem.* **4**, 276–285 (1923).
7. A. P. Steynberg, M. E. Dry, Fischer-Tropsch Technology (Elsevier, 2004), vol. 152, 722 pp.
8. R. B. Anderson, H. Kölbel, M. Rálek, *The Fischer-Tropsch Synthesis* (Academic Press, 1984).
9. M. E. Dry, J. C. Hoogendoorn, Technology of the Fischer-Tropsch process. *Catal. Rev. Sci. Eng.* **23**, 265–278 (1981).
10. C. G. Visconti, L. Lietti, P. Forzatti, R. Zennaro, Fischer–Tropsch synthesis on sulphur poisoned Co/Al_2O_3 catalyst. *Appl. Catal. A* **330**, 49–56 (2007).
11. A. Y. Khodakov, W. Chu, P. Fongarland, Advances in the development of novel cobalt Fischer–Tropsch catalysts for synthesis of long-chain hydrocarbons and clean fuels. *Chem. Rev.* **107**, 1692–1744 (2007).
12. M. E. Dry, in *Catalysis Science and Technology* (Springer Verlag, 1981), vol. 1, pp. 159–255.
13. M. E. Dry, in *Encyclopedia of Catalysis* (John Wiley & Sons, 2003), vol. 3, pp. 347–403.
14. M. Meinshausen, N. Meinshausen, W. Hare, S. C. B. Raper, K. Frieler, R. Knutti, D. J. Frame, M. R. Allen, Greenhouse-gas emission targets for limiting global warming to 2°C. *Nature* **458**, 1158–1162 (2009).
15. S. Chu, Carbon capture and sequestration. *Science* **325**, 1599 (2009).
16. R. J. Madon, W. F. Taylor, Fischer-Tropsch synthesis on a precipitated iron catalyst. *J. Catal.* **69**, 32–43 (1981).
17. J. W. Niemantsverdriet, A. M. Van der Kraan, W. L. Van Dijk, H. S. Van der Baan, Behavior of metallic iron catalysts during Fischer-Tropsch synthesis studied with Mössbauer spectroscopy, x-ray diffraction, carbon content determination, and reaction kinetic measurements. *J. Phys. Chem.* **84**, 3363–3370 (1980).
18. A. Königer, C. Hammerl, M. Zeitler, B. Rauschenbach, Formation of metastable iron carbide phases after high-fluence carbon ion implantation into iron at low temperatures. *Phys. Rev. B* **55**, 8143–8147 (1997).
19. E. de Smit, A. M. Beale, S. Nikitenko, B. M. Weckhuysen, Local and long range order in promoted iron-based Fischer–Tropsch catalysts: A combined in situ x-ray absorption spectroscopy/wide angle x-ray scattering study. *J. Catal.* **262**, 244–256 (2009).
20. E. de Smit, F. Cinquini, A. M. Beale, O. V. Safonova, W. van Beek, P. Sautet, B. M. Weckhuysen, Stability and reactivity of $\epsilon-\chi-\theta$ iron carbide catalyst phases in Fischer– Tropsch synthesis: Controlling μ_C. *J. Am. Chem. Soc.* **132**, 14928–14941 (2010).
21. M. D. Shroff, D. S. Kalakkad, K. E. Coulter, S. D. Kohler, M. S. Harrington, N. B. Jackson, A. G. Sault, A. K. Datye, Activation of precipitated iron Fischer-Tropsch synthesis catalysts. *J. Catal.* **156**, 185–207 (1995).
22. C. Yang, H. Zhao, Y. Hou, D. Ma, Fe_5C_2 nanoparticles: A facile bromide-induced synthesis and as an active phase for Fischer–Tropsch synthesis. *J. Am. Chem. Soc.* **134**, 15814–15821 (2012).
23. V. P. Santos, T. A. Wezendonk, J. José Delgado Jaén, A. Iulian Dugulan, M. A. Nasalevich, H.-U. Islam, A. Chojecki, S. Sartipi, X. Sun, A. A. Hakeem, A. C. J. Koeken, M. Ruitenbeek, T. Davidian, G. R. Meima, G. Sankar, F. Kapteijn, M. Makkee, J. Gascon, Metal organic framework-mediated synthesis of highly active and stable Fischer-Tropsch catalysts. *Nat. Commun.* **6**, 6451 (2015).
24. K. Xu, B. Sun, J. Lin, W. Wen, Y. Pei, S. Yan, M. Qiao, X. Zhang, B. Zong, ε-Iron carbide as a low-temperature Fischer–Tropsch synthesis catalyst. *Nat. Commun.* **5**, 5783 (2014).
25. K. H. Jack, Structural transformations in the tempering of high-carbon martensitic steels. *J. Iron Steel Inst.* **169**, 26–36 (1951).
26. S. Andersson, B. G. Hyde, Twinning on the unit cell level as a structure-building operation in the solid state. *J. Solid State Chem.* **9**, 92–101 (1974).
27. S. Nagakura, Study of metallic carbides by electron diffraction part III. Iron carbides. *J. Phys. Soc. Jpn.* **14**, 186–195 (1959).
28. G. Le Caër, J. M. Dubois, M. Pijolat, V. Perrichon, P. Bussiere, Characterization by Moessbauer spectroscopy of iron carbides formed by Fischer-Tropsch synthesis. *J. Phys. Chem.* **86**, 4799–4808 (1982).
29. J. Xu, C. H. Bartholomew, Temperature-programmed hydrogenation (TPH) and in situ Mössbauer spectroscopy studies of carbonaceous species on silica-supported iron Fischer– Tropsch catalysts. *J. Phys. Chem. B* **109**, 2392–2403 (2005).
30. S. Li, S. Krishnamoorthy, A. Li, G. D. Meitzner, E. Iglesia, Promoted iron-based catalysts for the Fischer–Tropsch synthesis: Design, synthesis, site densities, and catalytic properties. *J. Catal.* **206**, 202–217 (2002).
31. S. Krishnamoorthy, A. Li, E. Iglesia, Pathways for CO_2 formation and conversion during Fischer–Tropsch synthesis on iron-based catalysts. *Catal. Lett.* **80**, 77–86 (2002).
32. M. Ojeda, R. Nabar, A. U. Nilekar, A. Ishikawa, M. Mavrikakis, E. Iglesia, CO activation pathways and the mechanism of Fischer–Tropsch synthesis. *J. Catal.* **272**, 287–297 (2010).
33. H. Cheng, D. B. Reiser, S. Dean Jr., On the mechanism and energetics of Boudouard reaction at FeO (1 0 0) surface: $2CO \rightarrow C + CO_2$. *Catal. Today* **50**, 579–588 (1999).
34. J. Moon, V. Sahajwalla, Investigation into the role of the Boudouard reaction in self-reducing iron oxide and carbon briquettes. *Metall. Mater. Trans. B* **37**, 215–221 (2006).
35. T. A. Wezendonk, V. P. Santos, M. A. Nasalevich, Q. S. E. Warringa, A. Iulian Dugulan, A. Chojecki, A. C. J. Koeken, M. Ruitenbeek, G. Meima, H.-U. Islam, G. Sankar, M. Makkee, F. Kapteijn, J. Gascon, Elucidating the nature of Fe species during pyrolysis of the Fe-BTC MOF into highly active and stable Fischer–Tropsch catalysts. *ACS Catal.* **6**, 3236–3247 (2016).
36. Z. Klencsár, Mössbauer spectrum analysis by Evolution Algorithm. *Nucl. Instrum. Methods Phys. Res. B* **129**, 527–533 (1997).
37. J. R. Rostrup-Nielsen, Production of synthesis gas. *Catal. Today* **18**, 305–324 (1993).
38. Y. V. Maksimov, I. P. Suzdalev, R. A. Arents, S. M. Loktev, Mössbauer study of iron carbides formed on a fused iron catalyst in the synthesis of higher alcohols from carbon monoxide and hydrogen. *Kinet. Catal.* **15**, 1293 (1974).
39. G. B. Raupp, W. N. Delgass, Mössbauer investigation of supported Fe and FeNi catalysts: II. Carbides formed Fischer-Tropsch synthesis. *J. Catal.* **58**, 348–360 (1979).

Acknowledgments: We acknowledge colleagues from the National Institute of Clean-and-Low-Carbon Energy (NICE) in China: Y. Lv for R-Fe preparation, Z. Men and Q. Sun for the CTL process discussion, and F. Zhang and T. Wang for general assistance. We also acknowledge T. F. Kimpel from Eindhoven University of Technology for the FT tests. **Funding:** This work was supported by the National Key Research and Development Program of China (no. 2017YFB0602500). E.J.M.H. received financial support through a NWO-Top grant awarded by the Netherlands Organization for Scientific Research. **Author contributions:** P.W. conceived the idea of catalyst synthesis and designed and carried out the experiments. W.C. designed, performed, and interpreted the experiments and wrote the manuscript in consultation with P.W. E.J.M.H. supervised the project and contributed to the design and interpretation of the experiments. F.-K.C. and Y.S. contributed to the environmental TEM experiments. A.I.D. performed and interpreted the Mössbauer experiments. R.P. assisted in writing and contributed to data interpretation. K.Z. carried out catalytic tests. J.Y. contributed to ASPEN simulation. B.F. contributed to XRD. P.M. and W.X. guided the discussion on the CTL process and the energy strategy. All the authors contributed to discussion and commented on the manuscript. **Competing interests:** The authors declare that they have no competing interests. **Data and materials availability:** All data needed to evaluate the conclusions in the paper are present in the paper and/or the Supplementary Materials. Additional data related to this paper may be requested from the authors.

Submitted 25 May 2018
Accepted 5 September 2018
Published 12 October 2018
10.1126/sciadv.aau2947

Citation: P. Wang, W. Chen, F.-K. Chiang, A. I. Dugulan, Y. Song, R. Pestman, K. Zhang, J. Yao, B. Feng, P. Miao, W. Xu, E. J. M. Hensen, Synthesis of stable and low-CO_2 selective ε-iron carbide Fischer-Tropsch catalysts. *Sci. Adv.* **4**, eaau2947 (2018).